Applied Thermal Engineering 42 (2012) 34–40

Contents lists available at SciVerse ScienceDirect

Applied Thermal Engineering

journal homepage: www.elsevier.com/locate/apthermeng

Experimental investigation of loop heat pipe with flat evaporator using biporous wick

B.B. Chen, W. Liu*, Z.C. Liu*, H. Li, J.G. Yang

School of Energy and Power Engineering, Huazhong University of Science and Technology, 415 Power Building, 1037 Luoyu Road, Hongshan District, Wuhan 430074, China

ARTICLE INFO

Article history:
Received 9 December 2011
Accepted 6 March 2012
Available online 13 March 2012

Keywords:
Loop heat pipe
Flat evaporator
Biporous wick
Evaporator temperature
Heat flux
Electronic cooling

ABSTRACT

In order to solve heat dissipation of electronic equipment, an experimental investigation was carried out on the thermal performance of a miniature stainless-steel-ammonia loop heat pipe (LHP) with a flat disk-shaped evaporator. A biporous wick made from nickel powder was used for developing the capillary force. Tests demonstrated that the device could start up at heat load as low as 2.5 W. Meantime, the maximum heat load the LHP could transfer reaches 130 W (heat flux 12.8 W/cm^2) at the allowable evaporator temperature of below 60 °C. The LHP showed a very fast response to variable heat load and operated stably without obvious temperature oscillation. The evaporator surface has very high isothermality while the monitored temperature difference between the maximum and minimum value on the evaporator surface does not exceed 3 °C for heat load below 130 W. The operation modes of variable conductance and constant conductance are found in the whole tested heat load range. The total thermal resistance varies between 1.42 and 0.33 °C/W at heat load ranging from 10 to 130 W.

1. Introduction

In recent decades, some two-phase devices have been developed for solving the thermal control of electronic devices with high heat flux and limited space. Loop heat pipe (LHP) is an efficient two-phase device which is based on the evaporation and condensation of working fluid to transfer heat. The working fluid is circulated by capillary force developed in the fine porous wick. LHP offers many advantages over traditional heat pipes, including high heat transfer capability, flexible transport lines and heat transfer over long distances.

Since LHP is first proposed in the early 1980's [1], many researchers have studied the operating principle of the LHP experimentally and theoretically [2–4]. The main components of LHP include evaporator, compensation chamber (CC), condenser, vapor and liquid lines. Among all the existing LHP designs, the evaporators are designed into cylinder or plate shapes. As most heat sources have flat thermo-contact surfaces, the cylindrical evaporator needs a saddle to locate at the evaporator surface. This configuration has disadvantages of increasing the thermal resistance and the mass of the body. The flat evaporator does not have these problems mentioned above. As the electronic devices are miniaturized, LHP with flat evaporator is more adapted to electronic cooling applications [5]. Meantime, due to the liquid evaporating uniformly on the flat surface, the LHP with flat evaporator has very high isothermality among the two-phase cooling systems.

Several different flat evaporator configurations in LHP have been investigated. Maidanik et al. [6] tested a LHP with a flat disc-shaped evaporator at horizontal and vertical orientations. The thermal resistance varied in the range from 1.05 to 0.42 °C/W at heat load from 40 to 80 W. Tu et al. [7] developed an overall two-dimensional numerical model to address the heat and mass transfer characteristics in the evaporator and investigated the start-up characteristics of a LHP with flat evaporator experimentally. A flat-oval evaporator with a finned radiator equipped on the CC was designed by Becker et al. [8] to reduce the LHP operating temperature. The minimum thermal resistance of the LHP was 0.2 °C/W for a heat load of 100 W. The thermal performance of the LHP is related to the working fluid, fluid inventory, elevation and heat sink temperature. Liu et al. [9] investigated the effects of different working fluids, methanol and acetone, on the operating characteristic of LHP with flat evaporator. Joung et al. [10,11] developed a LHP with a thin planar bifacial evaporator to examine its operating characteristics at different fluid inventories, elevations and heat sink temperatures. The maximum heat flux at allowable evaporator temperature is very important for the electronic cooling. A miniature copper-water LHP with flat disk-shaped evaporator designed by Singh et al. [12] was able to transfer the maximum heat load of 70 W with the evaporator temperature

* Corresponding authors. Tel.: +86 27 87542618; fax: +86 27 87540724.
E-mail addresses: w_liu@hust.edu.cn (W. Liu), zcliu@hust.edu.cn (Z.C. Liu).

1359-4311/$ – see front matter © 2012 Elsevier Ltd. All rights reserved.
doi:10.1016/j.applthermaleng.2012.03.006

Nomenclature

Q	heat load (W)
R	thermal resistance (°C/W)
T	temperature (°C)
ΔT	temperature difference (°C)

Subscripts

cond	condenser
evap	evaporator
sink	heat sink

Abbreviations

Amb	the ambient air
CC	compensation chamber
Cond-in	condenser inlet, TC 7
Cond-out	condenser outlet, TC 8
Comp-wall	compensation chamber wall, TC 11
Evap	evaporator wall/evaporator, TC 1–4
Evap-in	evaporator inlet, TC 10
Evap-out	evaporator outlet, TC 5
TC	thermocouple

below 100 °C. Celata et al. [13] reported that a stainless-steel-water LHP with flat evaporator could transfer a maximum heat load of 75 W with the evaporator temperature below 150 °C in the favorable configuration. Among these investigations mentioned above, the evaporator temperatures are too high at high heat flux. These devices are limited to apply to heat dissipation in the electronic equipment with high heat flux.

The wick structure is a very critical component for the LHP. Wicks with bimodal pore size distributions were utilized to improve the heat transfer capability of the LHPs. Yeh et al. [14,15] studied the evaporative heat transfer of biporous wicks with various bimodal pore size distributions. The experimental results showed that the heat transfer coefficient of the biporous wick reached a maximum value of 64 000 $W/m^2 \cdot K$ at the heat sink temperature of 10 °C and the evaporator temperature of 85 °C. Semenic et al. [16] firstly based correlations for thermophysical properties of biporous media on distribution means of clusters and particles. They compared the thermophysical properties of monoporous wicks with various characteristic pore sizes as well as biporous wicks with various thicknesses experimentally [17]. Wang and Catton [18] proposed that the biporous structure improved the vapor and liquid distribution in the porous media and the biporous heat pipe is more attractive than the monoporous and the solid copper spreader for high power electronic device cooling. Although much work has been noted that biporous wick could improve the heat transfer performance for heat pipes, there are rare literatures about biporous wick used in the LHP with flat evaporator.

When the evaporator is designed in the shape of miniature flat plate, the temperature oscillation could occur easily. The possible reasons for this oscillation refer to the configuration of the evaporator and the thermophysical property of the wick structure [19,20]. In this work, a biporous wick was used in the flat evaporator. 60 °C was the maximum allowable evaporator temperature for electronic equipment in our original intention. The goal of this investigation is to reveal the detailed characteristics of the LHP with flat evaporator during start-up and steady operation. Meantime, this investigation leads to a better understanding of biporous wick improving the thermal performance of the LHP with flat evaporator.

2. Experimental prototype and test process

2.1. The biporous wick structure

A biporous wick was used to generate the capillary force as well as to supply the working fluid for evaporation. For the fabrication method introduced in Ref. [15], small pores could be generated by sintering metal powder, while large pores could be formed by dissolving the pore formers. Sodium carbonate (Na_2CO_3) was chosen as the pore former. The pore former was mixed uniformly with nickel powder by a V-type mixer. Then the mixed powder was filled in a mold and pressed under the forming pressure. Afterward, the wick was seceded from the mold and sintered in a furnace. Hydrogen was used as the protective atmosphere. After that, the wick was cleaned by distilled water in an ultrasonic cleaner until Na_2CO_3 was washed away cleanly. Finally, the wick was dried out in an oven. Table 1 gives the sintering parameters of the biporous wick.

Fig. 1 shows the appearance and scanning electron microscopy (SEM) photographs of the biporous wick. Several small pores are seen between the nickel particles, and large pores are seen between the clusters. The large pores reduce the flow resistance and enhance the liquid transport and the vapor escape from the wick. The small pores continue to function as liquid supply pump developing the capillary force. Also, the biporous wick increases the evaporating surface area. So the bimodal pore size distributions allow the biporous wick to yield excellent hydrodynamic performance.

Porosity, permeability and effective pore radius are key parameters impacting on the performance of the LHP. The porosity and permeability are measured by experimental methods [21,22]. The measured porosity is open porosity which represents interconnected pores. The uncertainty analyses of the porosity and permeability are estimated to be within ±0.64% and ±8.4% respectively. The effective pore radius and the pore size distribution are analyzed using the image analysis method. The parameters of the porous wick are shown in Table 2.

2.2. LHP design and test methods

The experimental setup comprises a LHP system, a heating system, a cooling system and a measurement system, as presented in Fig. 2. The experimental apparatus except the LHP prototype has been described in our earlier work [23]. The flat evaporator configuration is shown in Fig. 3. The CC is designed for collecting the liquid returning from the condenser and storing the NCGs which may exist in the loops [24]. There are some vapor removal channels for the generated vapor moving towards vapor chamber smoothly. Meanwhile, the fins are used for transferring heat to the surface of the wick. The whole evaporator is jointed by laser welding. The condenser is a double-pipe heat exchanger, which condense the vapor and provide more sufficient subcooling to the liquid. A charging line is fixed on the liquid line for charging the working fluid. The condenser and the liquid line are insulated using efficient thermal insulation material (PVC/NBR, Fuerda, thermal conductivity 0.034 W/m·K). All components of the LHP are made of stainless steel except the outer pipe of the condenser which is made of copper. Table 2 presents main parameters of the LHP.

Table 1
The sintering parameters of the biporous wick.

Component	Particle size (μm)	Volume content (%)	Forming pressure (MPa)	Sintering temperature (°C)
Nickel	2.2–2.8	70	5	700
Na_2CO_3	<53	30		

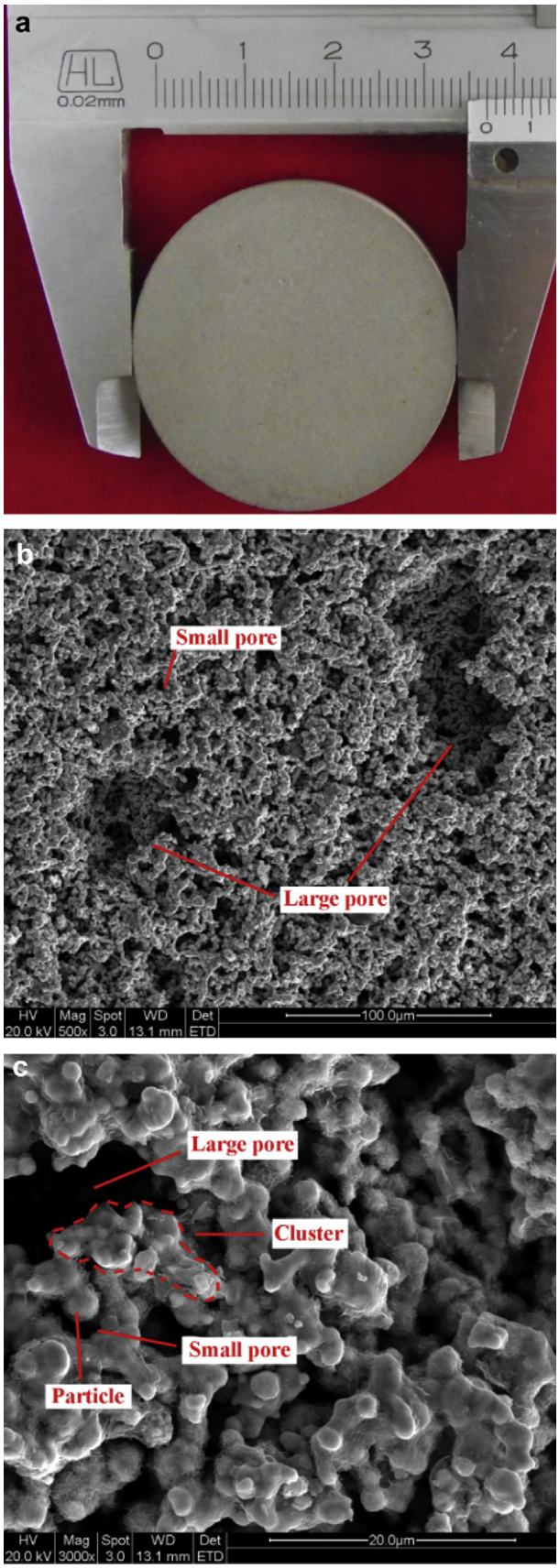

Fig. 1. Photographs of the biporous wick with bimodal pore size distributions. (a) The appearance of the wick. (b) SEM photograph (500-times). (c) SEM photograph (3000-times).

Table 2
The main parameters of the LHP.

Evaporator	
Diameter (mm)	43
Thickness (mm)	15
Compensation chamber diameter (mm)	40
Porous wick	
Diameter (mm)	37
Thickness (mm)	4
Porosity (%)	69
Porous radius (μm)	2.6–53
Permeability (m^2)	1.0×10^{-12}–1.4×10^{-12}
Vapor line length (mm)	335
Liquid line length (mm)	415
Vapor/liquid line diameter (mm)	2
Condenser length (mm)	960

Ammonia is used as the working fluid. Liquid charge ratio is a key parameter for reliable start-up and operation of the LHP. For lower liquid charge ratio, the wick dries out easily for lack of the liquid. For higher liquid charge ratio, the active condenser area is not sufficient for heat removal. Considering these two aspects, the liquid charge ratio is selected at 65% of the loop internal volume in the present experiment.

Fig. 4 shows the locations of T-type thermocouples, including the heater wall, the evaporator inlet and outlet, the CC wall, the condenser inlet and outlet, and the middle positions of the liquid and vapor lines. The evaporator temperature is presented by the temperature measured on the top surface of the heater. The accuracy of thermocouple is ±0.2 °C. The LHP is tested in the horizontal orientation with the evaporator and the condenser at the same elevation. In all tests, the ambient temperature is around 18 °C.

3. Results and discussions

3.1. Evaporator temperature difference

Isothermal evaporation is an important feature of the LHP with flat evaporator. Four thermocouples are attached to the evaporator to monitor its isothermality, as shown in Fig. 4(b). Temperature difference between these four positions is defined as:

$$\Delta T = T_{TCi} - T_{evap} \quad (1)$$

where T_{TCi} is the temperature measured by the thermocouple TC i (i = 1, 2, 3, 4), and T_{evap} is the average temperature of the evaporator.

The temperature differences of the evaporator at different heat loads are given in Fig. 5. The axis lying in the middle of the figure represents the average value. The obtained results show that the temperature difference augments with increasing heat load. The absolute value of temperature difference ranges from 0.2 °C at heat load of 2.5 W to 1.5 °C at heat load of 130 W. It could be inferred that the monitored temperature difference between the maximum and minimum value on the evaporator surface does not exceed 3 °C when heat load is below 130 W.

3.2. Start-up tests

One important aspect to evaluate the reliability and stability of the LHP is related with start-up behavior. Fig. 6 shows the start-up process of the LHP with a heat load of 100 W at the heat sink temperature of −15 °C. The evaporator temperature rises immediately as soon as heat load is applied to the evaporator active zone. Subsequently, both the temperatures of the evaporator outlet and

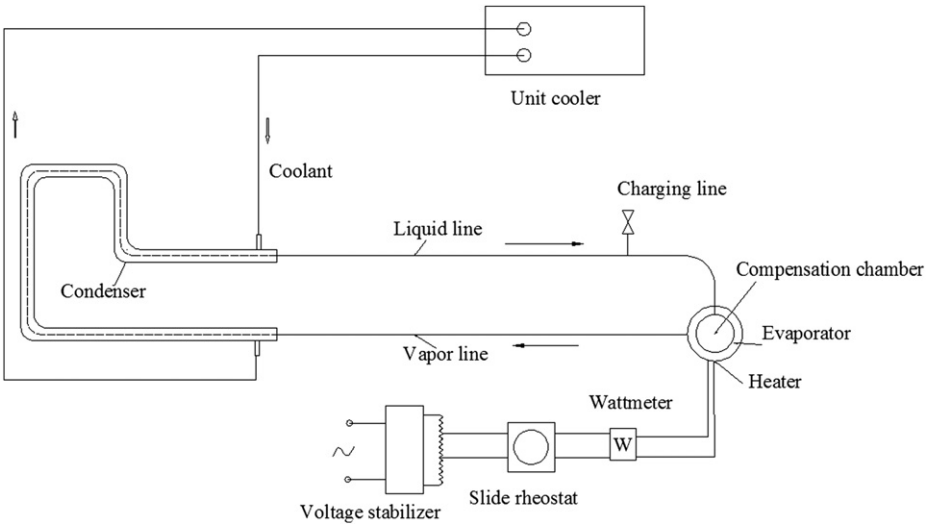

Fig. 2. The design and test schematic of the experimental prototype.

the condenser inlet increase quickly. That means the liquid inside the evaporator starts evaporating. As the vapor accumulates more, the evaporating meniscus is formed at the interface of the porous wick, which develops the capillary force to circulate the working fluid around the loop. The circulation does not start until the capillary force is larger than the total pressure drops of the system. The vapor moves along the vapor line to the condenser. In the condenser, the vapor is condensed and the liquid is subcooled. The liquid flows towards the CC through the liquid line. The CC temperature is decided by heat exchange with the evaporator, the ambient and the liquid returning from the condenser [2]. When energy balances for all loop elements are satisfied, the LHP reaches steady state. At last, the capillary force is equal to the total pressure drops.

From the curves of Fig. 6, the LHP starts up very rapidly within a period of 4 min. The whole process is very smooth without obvious temperature oscillation. During the start-up process, there is a slight temperature overshoot, which could be attributed to time delay required for the subcooled liquid to reach the CC [25]. It should be mentioned that no obvious temperature oscillation were observed in all tests except at heat load lower than 5 W. It is apparent that the biporous wick with low thermal conductivity could reduce the heat loss to the CC.

Fig. 7 presents a successful start-up with a heat load as low as 2.5 W. Both the condenser outlet temperature and the evaporator inlet temperature have obvious decrease after heat load is applied to the evaporator active zone. That means the liquid starts to flow back to the CC and the circulation of the working fluid is formed. Due to the sufficient subcooling of the liquid, the LHP could operate below the ambient temperature. There are slight temperature oscillations occurring at condenser outlet and evaporator inlet, which are caused by the pressure fluctuation in the two-phase zone in the condenser. Especially for small mass flow rate of the liquid at low heat load, the fluctuation effect on the liquid in the liquid line is obvious.

3.3. Operating characteristic of LHP

The temperature indicated in the following is measured at steady state. Fig. 8(a) and (b), respectively, present the main results of the tests in form of the temperature against heat load at the heat sink temperature of −15 and 0 °C. The LHP could start up at heat load as low as 2.5 W. The maximum heat load reaches 130 W (heat flux 12.8 W/cm^2) at the heat sink temperature of −15 °C or 120 W (11.8 W/cm^2) at the heat sink temperature of 0 °C when the evaporator temperature does not exceed 60 °C. From the flattened operating curve of the LHP, two operating modes consisting of variable conductance and constant conductance are observed [26]. For heat load less than 100 W ($T_{sink} = -15$ °C) or 80 W ($T_{sink} = 0$ °C), the LHP operates at variable conductance mode. In this case the CC temperature is decided by two main factors. One is the amount of the subcooling liquid returning from the condenser, the other one is the heat leak from the evaporator to the CC if not considering the heat exchange between it and the ambient. The heat leak is nearly compensated by the liquid subcooling, which cause no obvious temperature change of the CC with increasing heat load. Meantime, due to a majority of liquid staying in the condenser, the CC is partially filled with liquid. As the two-phase zone in the condenser

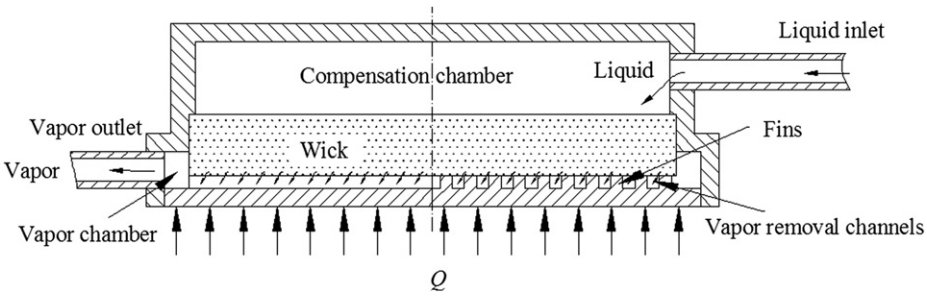

Fig. 3. The configuration of the evaporator.

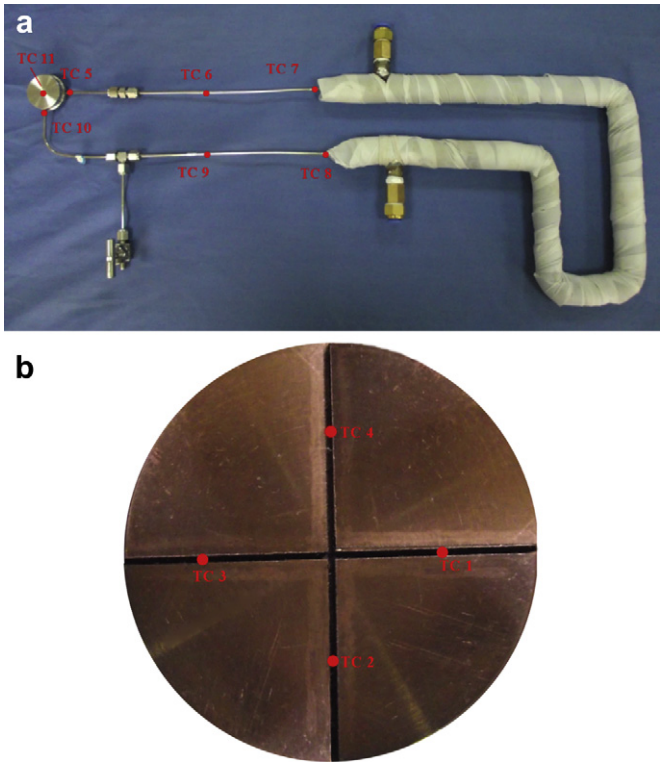

Fig. 4. The photographs of experimental setup and the fixed locations of the thermocouples. (a) The LHP. (b) The heater.

increases with increasing heat load, the liquid moves to the CC. The variable conductance mode continues until the CC is completely filled with liquid and the heat leak to the CC is larger than the liquid cooling from the condenser. For heat load more than 100 W ($T_{sink} = -15$ °C) or 80 W ($T_{sink} = 0$ °C), the LHP operates at constant conductance mode. Different heat sink temperatures impact the subcooling of the liquid and the operating temperature of the LHP. So the evaporator temperature at the heat sink temperature of −15 °C is lower than that at the heat sink temperature of 0 °C.

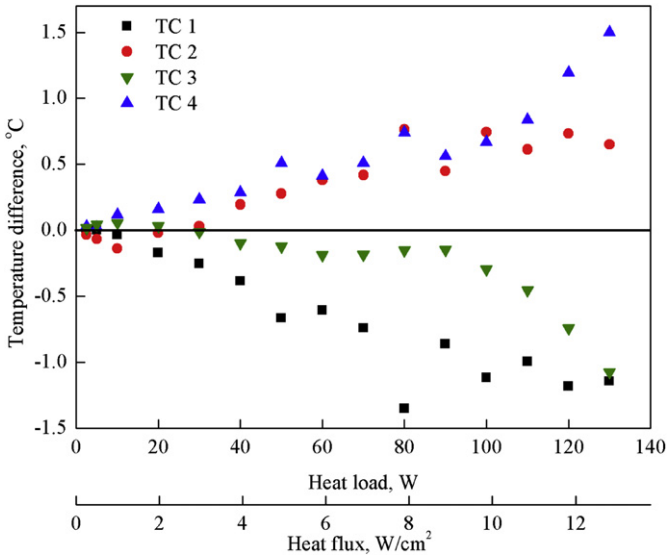

Fig. 5. Temperature differences of the evaporator at the heat sink temperature of −15 °C.

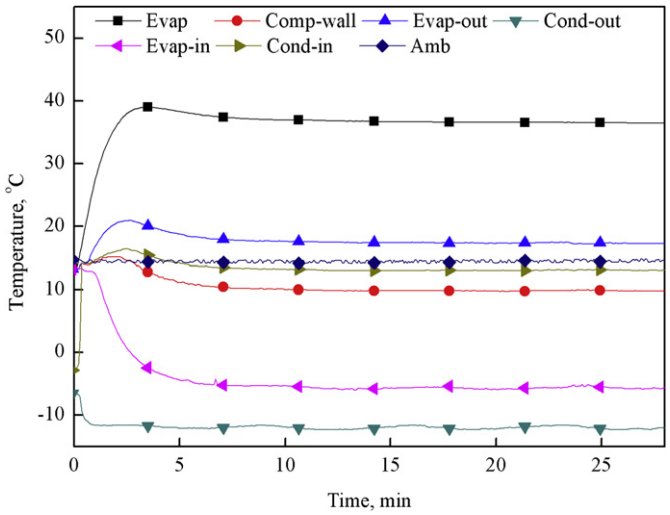

Fig. 6. Start-up of the LHP with a heat load of 100 W at the heat sink temperature of −15 °C.

3.4. Variable heat load tests

Another important aspect to evaluate the reliability and stability of the LHP is related with operating behavior with variable heat load. The LHP started up from the cold state at a certain heat load. When it reached steady state, the input power was changed in regular or random steps between 10 and 130 W and kept at least 25 min, which imitated different cycles of variable heat load.

Fig. 9(a) and (b), respectively, show the characteristics of transient operation with heat load cycles of 10-40-80-130-100-70-110-50-20-60-30 W and 70-30-80-110-90-60-20-120-50-40-10 W in sequential order. It is observed from the figures that the LHP shows a fast response to heat load when input power is switched. For each change, the steady state is achieved within short period of 2–7 min. During the whole cycle, the LHP presents a steady and smooth operation. Meanwhile, no obvious temperature oscillation and overshoot phenomena are found. Whatever heat load is changed in regular or random steps, the LHP is demonstrated to have a high performance of adjusting to heat load change.

3.5. Thermal resistance

The thermal resistance is calculated to assess the thermal performance of the LHP. The total thermal resistance of the LHP is defined as:

$$R_{LHP} = (T_{evap} - T_{cond})/Q \quad (2)$$

where, T_{evap} is the average temperature of the evaporator, which is measured by the thermocouples fixed on the surface of the heater (TC 1, 2, 3, 4). T_{cond} is the average temperature of the condenser, which is calculated by the thermocouples fixed at the condenser inlet (TC 7) and the condenser outlet (TC 8). Q is input power. The uncertainty analysis of R_{LHP} is estimated to be within ±11.6% at low heat load ($Q < 10$ W) and ±6.4% at high heat load ($Q > 10$ W).

The total thermal resistances of the LHP for different heat sink temperatures are presented in Fig. 10. It shows a typical trend of decreased thermal resistance of the LHP with increasing heat load. But when heat load is higher than 100 W, the total thermal resistance augments slightly with increasing heat load, as shown in the enlarged view of A zone in Fig. 10. For high heat load, as the heat leak through the wick becomes huge, some small bubbles form and coalesce in the wick which could block some paths for transferring

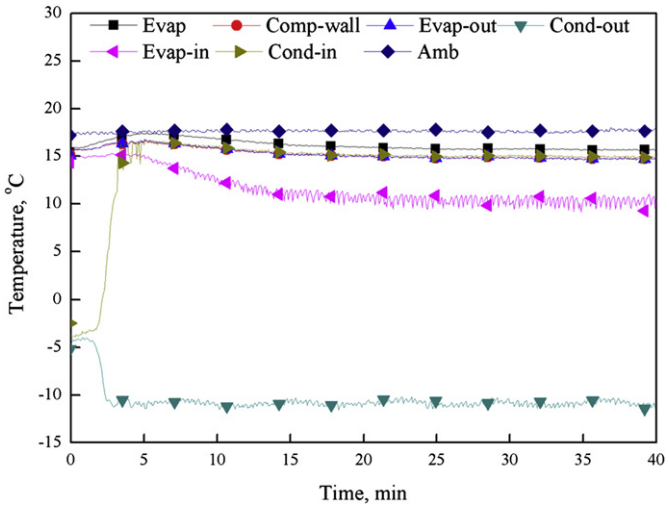

Fig. 7. Start-up of the LHP with a heat load of 2.5 W at the heat sink temperature of −15 °C.

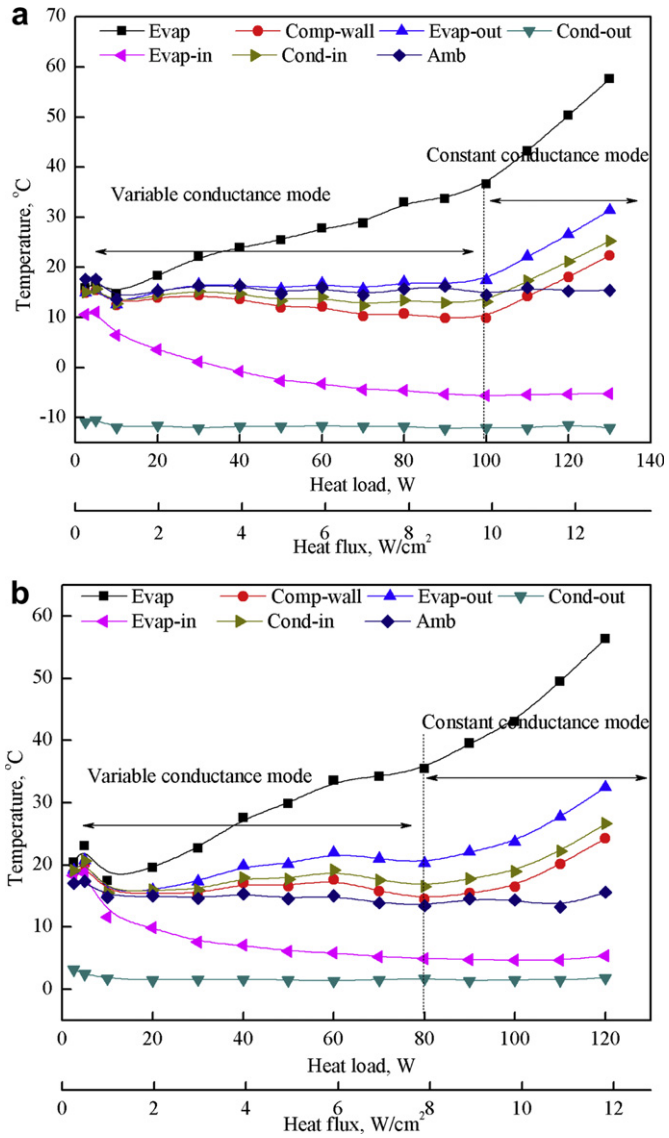

Fig. 8. The operating temperatures of characteristic points at different heat loads. (a) $T_{sink} = -15$ °C. (b) $T_{sink} = 0$ °C.

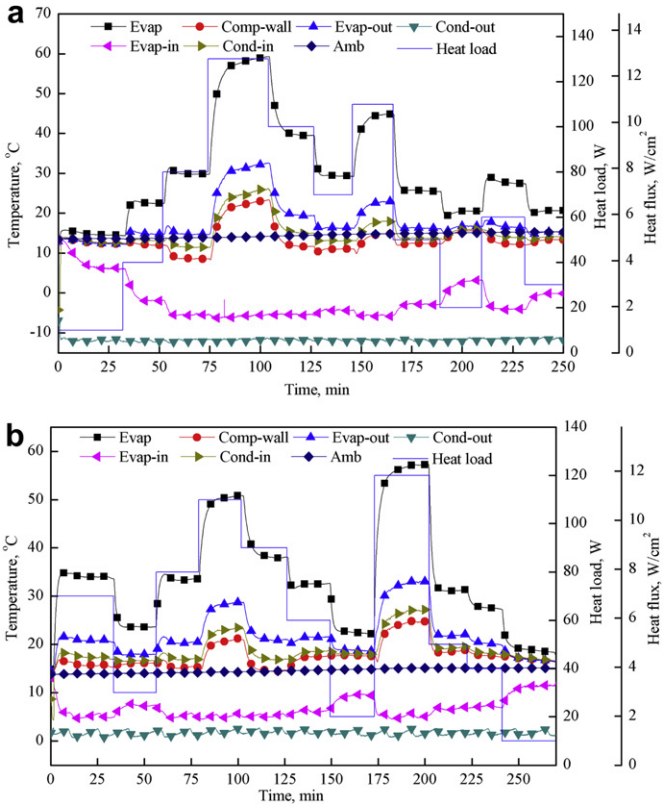

Fig. 9. The operating tests of the LHP for heat load changing in regular or random steps between 10 and 130 W. (a) $T_{sink} = -15$ °C. (b) $T_{sink} = 0$ °C.

liquid. Due to the weak hydrodynamic characteristic of the wick and the large heat leak to the CC at heat load of greater than 100 W, the thermal performance of the LHP decreases slightly. Thus, there is a slight increase at the total thermal resistance. The total thermal resistance, if not including the values below 10 W, varies in the range between 1.42 and 0.33 °C/W. Due to the increased temperature difference between the evaporator and the condenser, the total thermal resistance increases with decreasing the heat sink

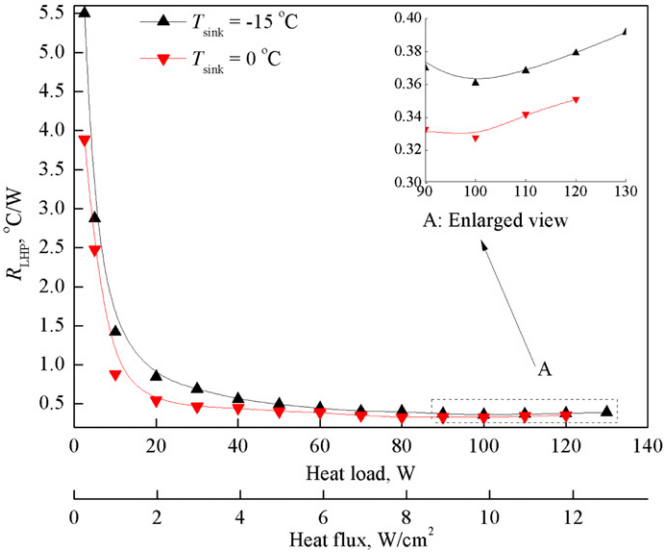

Fig. 10. The total thermal resistances of the LHP at two heat sink temperatures of −15 and 0 °C.

temperature. Also the effect of heat sink temperature on the total thermal resistance is analyzed by other authors [25].

4. Conclusions

In this article, a miniature stainless-steel-ammonia LHP with flat disk-shaped evaporator using biporous wick is investigated experimentally. The heat transfer performance of the LHP has been analyzed in detail, and the following conclusions can be drawn from the extensive experimental tests as follows:

1. The LHP could start up at heat load as low as 2.5 W. When the evaporator temperature does not exceed 60 °C, the maximum heat load the LHP could transfer reaches 130 W (heat flux 12.8 W/cm^2) at the heat sink temperature of −15 °C.
2. The evaporator surface has very high isothermality. The monitored temperature difference between the maximum and minimum value on the evaporator surface does not exceed 3 °C when heat load is below 130 W.
3. No obvious temperature oscillation and overshoot phenomena were observed during start-up and operation with variable heat load.
4. The operation modes of variable conductance and constant conductance are observed in the whole working heat load region.
5. When heat load ranges from 10 to 130 W, the total resistance of the LHP varies between 1.42 and 0.33 °C/W.

Acknowledgements

The current research was supported by the National Natural Science Foundation of China (Grant Nos. 50876035, 50906026, 51036003).

References

[1] Y.F. Maidanik, S. Vershinin, V. Kholodov, J. Dolgirev, Heat Transfer Apparatus, US Patent No. 4515209, 1985.
[2] J. Ku, Operating Characteristics of Loop Heat Pipes (1999) SAE Paper No. 1999-01-2007.
[3] Y.F. Maydanik, Review: loop heat pipes, Appl. Therm. Eng. 25 (2005) 635–657.
[4] S. Launay, V. Sartre, J. Bonjour, Parametric analysis of loop heat pipe operation: a literature review, Int. J. Therm. Sci. 46 (2007) 621–636.
[5] Y.F. Maydanik, Miniature loop heat pipes, in: Proceedings of the 13th International Heat Pipe Conference (2004), pp. 23–25 Shanghai, China.
[6] Y.F. Maidanik, S.V. Vershinin, M.A. Chernysheva, Development and Tests of Miniature Loop Heat Pipe with a Flat Evaporator (2000) SAE Paper No. 2000-01-2491.
[7] Z.K. Tu, Z.C. Liu, D.X. Gai, Z.M. Wan, W. Liu, Heat and mass transfer in a flat disc-shaped evaporator of a miniature loop heat pipe, Proc. Inst. Mech. Eng., Part G: J. Aerospace Eng. 223 (2009) 609–617.
[8] S. Becker, S. Vershinin, V. Sartre, E. Laurien, J. Bonjour, Y.F. Maydanik, Steady state operation of a copper-water LHP with a flat-oval evaporator, Appl. Therm. Eng. 31 (5) (2011) 686–695.
[9] Z.C. Liu, D.X. Gai, H. Li, W. Liu, J.G. Yang, M.M. Liu, Investigation of impact of different working fluids on the operational characteristics of miniature LHP with flat evaporator, Appl. Therm. Eng. 31 (16) (2011) 3387–3392.
[10] W. Joung, T. Yu, J. Lee, Experimental study on the loop heat pipe with a planar bifacial wick structure, Int. J. Heat Mass Transfer 51 (2008) 1573–1581.
[11] W. Joung, T. Yu, J. Lee, Experimental study on the operating characteristic of a flat bifacial evaporator loop heat pipe, Int. J. Heat Mass Transfer 53 (2010) 276–285.
[12] R. Singh, A. Akbarzadeh, M. Mochizuki, Operational characteristics of a miniature loop heat pipe with flat evaporator, Int. J. Therm. Sci. 47 (11) (2008) 1504–1515.
[13] G.P. Celata, M. Cumo, M. Furrer, Experimental tests of a stainless steel loop heat pipe with flat evaporator, Exp. Therm. Fluid Sci. 34 (2010) 866–878.
[14] C.C. Yeh, B.H. Liu, Y.M. Chen, A study of loop heat pipe with birpous wicks, Heat Mass Transfer 44 (2008) 1537–1547.
[15] C.C. Yeh, C.N. Chen, Y.M. Chen, Heat transfer analysis of a loop heat pipe with biporous wicks, Int. J. Heat Mass Transfer 52 (2009) 4426–4434.
[16] T. Semenic, Y.Y. Lin, I. Catton, Thermophysical properties of biporous heat pipe evaporators, ASME J. Heat Transfer 130 (2) (2008) Paper No. 022602.
[17] T. Semenic, I. Catton, Experimental study of biporous wicks for high heat flux applications, Int. J. Heat Mass Transfer 52 (2009) 5113–5121.
[18] J.L. Wang, I. Catton, Biporous heat pipes for high power electronic device cooling, in: Proceedings of the 17th Semiconductor Thermal Measurement and Management Symposium (2001), pp. 211–218 San Jose, CA.
[19] J. Li, D. Wang, G.P. Peterson, Experimental studies on a high performance compact loop heat pipe with a square flat evaporator, Appl. Therm. Eng. 30 (2010) 741–752.
[20] D.X. Gai, W. Liu, Z.C. Liu, J.G. Yang, Experimental investigation of temperature oscillation of mLHP with flat evaporator, Heat Transfer Res. 40 (6) (2009) 321–332.
[21] G.M. Xin, K.H. Cui, Y. Zou, L. Chen, Development of sintered Ni–Cu wicks for loop heat pipes, Sci. China Ser. E-Technol. Sci. 52 (6) (2009) 1607–1612.
[22] Z.Q. Chen, P. Cheng, T.S. Zhao, An experimental study of two phase flow and boiling heat transfer in bi-dispersed porous channels, Int. Commun. Heat Mass Transfer 27 (3) (2000) 293–302.
[23] H. Li, Z.C. Liu, B.B. Chen, W. Liu, C. Li, Development of biporous wicks for flat-plate loop heat pipe, Exp. Therm. Flu. Sci. 37 (2012) 91–97.
[24] R. Singh, A. Akbarzadeh, M. Mochizuki, Operational characteristics of the miniature loop heat pipe with non-condensable gases, Int. J. Heat Mass Transfer 53 (2010) 3471–3482.
[25] Y. Chen, M. Groll, R. Mertz, Y.F. Maydanik, S.V. Vershinin, Steady-state and transient performance of a miniature loop heat pipe, Int. J. Therm. Sci. 45 (2006) 1084–1090.
[26] S. Launay, V. Sartre, J. Bonjour, Analytical model for characterization of loop heat pipes, J. Thermophys. Heat Transfer 22 (4) (2008) 623–631.